DOI 10.24425/aee.2025.155963

Comparative study on the performance of novel electromagnetic induction heating and electric heating turnout snow melting system

YUE SHE, QINGFENG WANG✉, JIANQIONG ZHANG, XIANGQIANG LI

School of Physical Science and Technology, Southwest Jiaotong University
No. 111, North Section 1 of the Second Ring Road, Chengdu, Sichuan, China
e-mail: 2226808788@qq.com, {✉ wangqingfeng173/qilinxing/xiangqiang_li}@163.com

(Received: 15.06.2025, revised: 03.11.2025)

Abstract: This study addresses the issues of high energy consumption and low efficiency in conventional electric heating snow-melting systems for railway turnouts. A novel system is proposed that integrates electromagnetic induction heating with traditional electric heating to optimise energy transfer pathways and enhance energy utilisation efficiency. The system enables dynamic adjustment of heating power, thereby supporting adaptive operation under varying environmental conditions. Through theoretical analysis, temperature field simulations, and experimental validation, the energy regulation mechanism and performance characteristics are examined. Results show that, under full snow-cover conditions, the proposed induction heating system reduces snow-melting time by 76.9% compared with traditional electric heating, while achieving a 29% efficiency gain under snow-free conditions. Steady-state temperature rise tests demonstrate close agreement between simulations and measurements: directional heat transfer efficiency improves significantly, with the average rail temperature decreasing by 8.5% and the air temperature in the working area increasing by 15%. Additionally, the system increases the ice- and snow-melting rates by 0.4 and 0.8 times, respectively, while reducing energy consumption by 30–40%. An optimised composite thermal structure further enhances heat utilisation. This study provides both theoretical and practical insights for advancing turnout snow-melting technology and its engineering applications.

Key words: electric heating of railway turnouts, energy saving, induction heating of turnouts, temperature field simulations

1. Introduction

As a fundamental component of railway track systems, the operational status of turnouts plays a critical role in ensuring the safety and punctuality of train operations. In high-latitude and cold regions, such as Siberia, Canada, Hokkaido in Japan, and the Swiss Alps, severe winter weather conditions frequently cause disruptions to switching functions [1]. The adverse effects of snowfall on switch conversion are manifested in four typical scenarios, as illustrated in Fig. 1, which can be broadly categorised into two main aspects.

Firstly, geometric effects arise from the accumulation of snow and ice on the contact surfaces between the base rail and the switch rail, preventing proper closure and alignment. Such geometric deviations may lead to train derailments or other serious safety incidents. Secondly, mechanical performance is compromised under low-temperature conditions, where ice formation on the closure or repulsion sides of the turnout increases frictional resistance during the switching process. This impairment reduces the turnout's ability to complete conversion as instructed [2, 3], thereby disrupting traffic scheduling and increasing the risk of train delays.

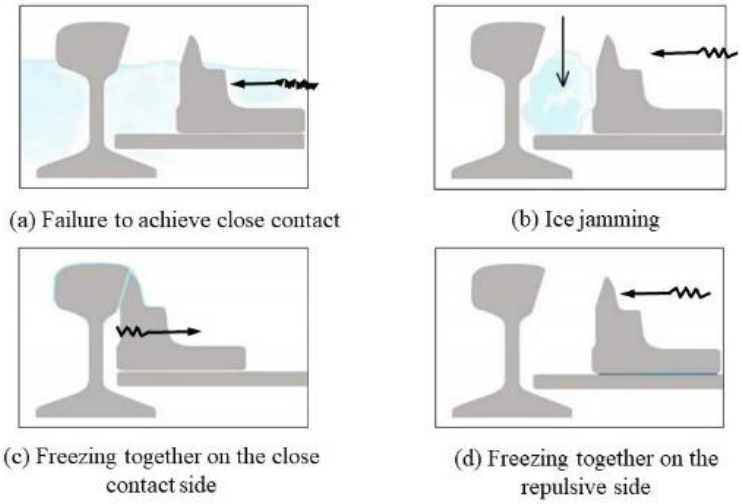

Fig. 1. Effects of snowfall on turnout operation

To address the aforementioned challenges and limitations of existing turnout snow-melting systems, this study proposes a novel system employing electromagnetic induction heating within a frequency range of 20 kHz to 50 kHz. The system enables efficient energy transfer and integrates a dynamic power adjustment mechanism, thereby supporting adaptive operation under varying environmental conditions. A comprehensive comparative analysis was conducted between the proposed system and conventional electric heating systems through theoretical modelling, temperature field simulations, and experimental validation. This multi-faceted assessment confirms the performance advantages of the proposed approach, providing both a solid theoretical foundation and practical guidance for the optimisation and engineering application of turnout snow-melting technology.

2. Overview of turnout snow-melting systems

2.1. Turnout snow melting technology

The primary methods for snow melting and de-icing on railway turnouts currently include manual operation, electric heating, gas heating, and cold air compression, as shown in Fig. 2. However, these traditional snow removal techniques exhibit low operational efficiency, complex system designs, and elevated safety risks [4]. Considering gas heating technology as an example, it delivers a high thermal power output of around 1 kW/m, but requires the construction of specialised gas supply infrastructure. Moreover, mechanical vibrations from train operations may induce gas leaks, potentially leading to explosions and posing significant safety hazards [5]. To ensure the reliable performance of turnout switching equipment during winter, an efficient and automated snow-melting system is essential. Upon snowfall, the system utilises its integrated intelligent monitoring module to detect snow conditions and promptly activates heating devices. This enables precise and effective snow removal from turnout surfaces while preventing secondary freezing through continuous temperature control. Such measures strongly support the uninterrupted functionality of turnout operations.

Fig. 2. Several types of turnout snow-melting systems in real life view

2.2. Energy efficiency challenges in electric-heated turnout snow-melting systems

Currently, the most widely adopted and highly automated turnout snow-melting system is the electric heating snow-melting system. Its operation relies on Joule's law, converting electrical current passing through specific resistive elements into heat energy, with a common heating power of 300–500 W/m. Heating strips are installed via specialised fixtures at key locations, including the base rail, the heart of the rail waist or rail slopes, the sliding bed plate, the outer locking frame, the closure checking device beneath the rod, and other accessible positions [6]. The heating strips maintain close contact with the rail. During operation, heat generated by the strips is conducted to the rail and snow, while convection and radiation effects disperse heat to the surrounding air medium. The rail subsequently transfers this heat to the snow and air, as illustrated in Fig. 3.

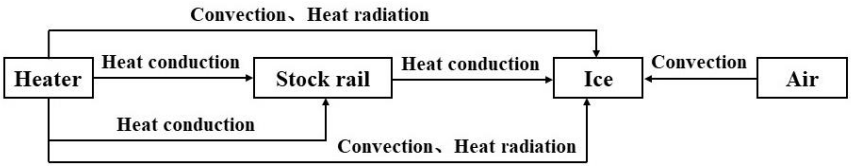

Fig. 3. The heat transfer process of turnout snow melting systems

The rail's large volume and specific heat capacity result in a relatively slow temperature rise. Meanwhile, the rate of heat dissipation to the air through radiation is rapid. This phenomenon causes the heat in specific sections of the base rail, as well as energy dissipated to the external environment, to be inadequately utilised for turnout snow melting, leading to significant heat energy wastage in non-working areas. Research by Flis M. *et al*. demonstrates that, under identical conditions, the spaced installation of resistance heating strips yields a significant improvement in snow-melting efficiency compared to their close-fitting installation. This finding further corroborates the theoretical analysis presented herein. Consequently, the traditional electric heating snow-melting system exhibits drawbacks, including high energy consumption and low snow-melting efficiency. Relevant data indicate that the power consumed by electric heating equipment accounts for approximately 40% of the total power demand of the railway transport system, substantially increasing operational costs [7].

2.3. Structural design of a novel electromagnetic induction heating turnout snow melting system

Induction heating technology utilises high-frequency alternating current to induce the skin effect, significantly increasing current density in the conductor's surface layer. This enables precise control of penetration depth at a microscopic level [8]. This physical phenomenon ensures rapid concentration of heat energy on the conductor's surface while offering advantages such as fast heating rates, high energy conversion efficiency, environmental friendliness, and non-contact operation. Its working principle is shown in Fig. 4. Consequently, it finds widespread application in metal processing, welding, food processing, medical fields, and beyond [9]. Addressing the need to optimise energy efficiency in railway turnout snow-melting systems, researchers have proposed integrating induction heating technology into existing devices. This approach achieves precise heat supply to critical turnout areas via directional heat conduction, mitigating the ineffective heat diffusion inherent in traditional electric heating methods [10]. Given the spatial constraints between the base rail and switch rail during close fitting, the heating element thickness is restricted to 10 mm or less.

The novel electromagnetic induction heating device developed in this study features a modular structure with geometry resembling conventional electric heating elements. As depicted in Fig. 5, the system consists of a multi-physics coupling unit, comprising four core components: an induction coil assembly (operating at a frequency of 20–50 kHz), an eddy current heat generation module, a magnetic flux guidance mechanism, and an electromagnetic shielding structure. Compared with the 250 kHz system reported in previous studies [11], this medium-frequency design reduces energy loss, improves thermal uniformity, and enhances electromagnetic compatibility. The design achieves adjustable heating power by regulating the excitation source current and frequency. Unlike induction heating methods that use tracks as heat sources, this design has better compatibility

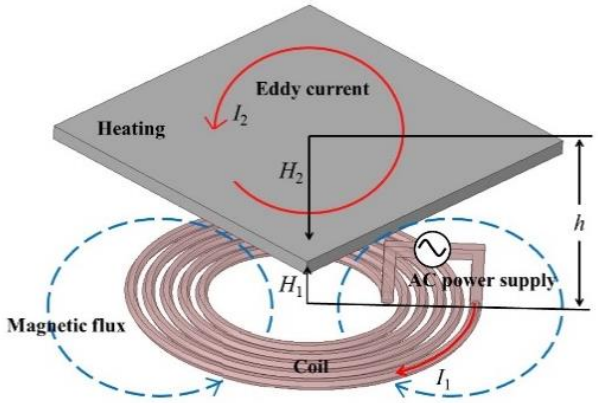

Fig. 4. Simplified schematic diagram of induction heating

with existing electric heating system fixtures and can adapt to the complex geometry of switches. This flexibility enables the system to optimise power based on environmental conditions, thereby achieving optimal operating performance and enhancing energy-saving potential.

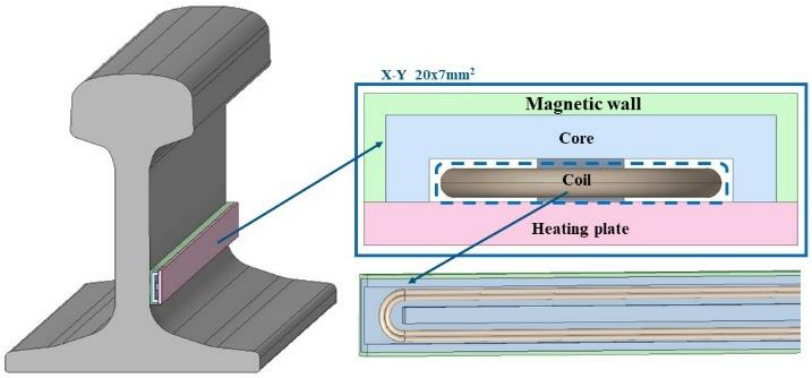

Fig. 5. Schematic diagram of the novel induction heater structure

The coil windings are crafted from copper-core enamelled wire to meet miniaturisation requirements, generating a directional alternating magnetic field via a high-frequency inverter circuit. In terms of energy conversion, the material properties of the eddy current effect heat generation module critically influence electromagnetic-thermal coupling efficiency. SUS 430 is selected as the preferred induction heating load material due to its superior magnetic permeability and electrical conductivity, enabling high-efficiency conversion from electromagnetic to thermal energy. During induction heating, the magnetic core's primary role is to concentrate the magnetic field on the heating plate, preventing outward dispersion of magnetic flux lines [11]. To achieve this, the core material must exhibit high permeability, low loss, and resistance to vibration in practical applications. Structurally, E-cores prove more effective at magnetic field concentration; thus, TDK PC95 series manganese-zinc ferrite, a soft magnetic material, is chosen. Its low thermal

conductivity forms an axial thermal resistance layer, reducing heat transfer to the rails. Additionally, to prevent magnetic field penetration from the device's base and protect other components [12], the magnetic shielding system employs Alnico permanent magnetic alloy to create a three-dimensional magnetic barrier, enhancing device safety and stability. Through finite element multiphysics field optimisation, the final compact heater achieves an effective working volume of 20×7 mm^2. Components are encapsulated and secured with epoxy resin, ensuring stable and reliable operation of the electromagnetic heater across diverse environments.

2.4. Heat transfer mechanism

Heat transfer is a physical phenomenon driven by temperature differences between two objects, primarily facilitated through three mechanisms: heat conduction, heat convection, and heat radiation. Within the turnout structure, heat transfer encompasses several dimensions: heat conduction within heating elements and rails, convective heat transfer between solids and air, radiative heat transfer between solids and the environment, and the heat required to melt snow [13].

2.4.1. Heat transfer

In the turnout snow-melting model, the heat transfer equation governs the heat exchange between solids in contact with the heater and the rail. According to Fourier's law, the thermal conductivity of the material directly influences heat transfer efficiency within the turnout structure.

$$q_{cd} = -k\nabla T, \tag{1}$$

where: q_{cd} is the conductive heat flux, W/m^2; k is the material thermal conductivity, W/(m·K); ∇T is the temperature gradient, K/m; and the negative sign indicates that the direction of heat transfer points in the direction of temperature decrease.

2.4.2. Heat convection

Upon activation of the heating device, heat conduction occurs within the turnout structure. Simultaneously, exposure to outdoor air induces convective heat transfer with the environment. In analysing the convective heat transfer of the turnout snow-melting model, this process is dynamically calculated, with Newton's cooling equation describing the heat exchange between solids and fluids.

$$q_{cn} = h\left(T_s - T_f\right), \tag{2}$$

where: h is the average convective heat transfer coefficient, W/(m^2·K); T_s is the solid surface temperature, K; T_f is the fluid temperature in contact with the solid, K. When the turnout structure carries out convective heat transfer with the ambient air, the wind speed v is a key factor affecting the size of the convective heat transfer coefficient h. Typically, under calm conditions with a wind power level of 0 and a wind speed of 0.1 m/s, the convective heat transfer coefficient h is set at 5 W/(m^2·K). This value establishes the convective heat transfer conditions between the solid and air. Initially, the temperatures of the solid (T_s) and fluid (T_f) are nearly equal. As heating progresses, the solid temperature rises, increasing the temperature difference and significantly enhancing convective heat transfer. Under windy conditions, the convective heat transfer effect becomes more pronounced.

2.4.3. Thermal radiation

Thermal radiation arises from the thermal motion of microscopic particles within an object, causing changes in charge distribution and electromagnetic oscillations, which subsequently emit electromagnetic waves outward. Any object with a temperature above absolute zero emits thermal radiation. The heat radiated by all objects is characterised within the radiative heat transfer model.

$$q_r = \varepsilon \sigma T^4, \tag{3}$$

where: ε is the solid surface emissivity coefficient, a constant; σ is the Stephen Boltzmann coefficient, W/(m^2·K^4); T is the surface temperature of the radiation object, K.

From Eq. (3), it can be seen that the emissivity of the object is linearly related to the radiative heat transfer, while the emissivity of the rails takes an approximate value of 0.17, and the radiative heat transfer is small, so more heat can be converged to the working area by increasing the radiative capacity.

The mathematical modelling of phase transitions, as an example of a highly nonlinear phenomenon, is very complex. When conduction, convection and the interface between snow and air are present, the model consists of the following equations, which together describe the physical phenomena and energy conversion mechanisms in the snow melting process at a turnout [14, 15].

2.4.4. Conservation of mass

$$\frac{\partial v_x}{\partial_x} + \frac{\partial v_y}{\partial_y} + \frac{\partial v_z}{\partial_z} = 0, \tag{4}$$

where v_x, v_y, v_z are velocities, m/s, and x, y, z are coordinates.

2.4.5. Conservation of momentum

$$\rho \frac{\partial v_x}{\partial_t} + \rho v_x \frac{\partial v_x}{\partial_x} + \rho v_y \frac{\partial v_x}{\partial_y} + \rho v_z \frac{\partial v_x}{\partial_z} = -\frac{\partial p}{\partial x} + \nabla \cdot (\mu \nabla v_x) + G_x + S_{vx} + F_{\sigma x}, \tag{5}$$

$$\rho \frac{\partial v_y}{\partial_t} + \rho v_x \frac{\partial v_y}{\partial_x} + \rho v_y \frac{\partial v_y}{\partial_y} + \rho v_z \frac{\partial v_y}{\partial_z} = -\frac{\partial p}{\partial y} + \nabla \cdot \left(\mu \nabla v_y\right) + G_y + S_{vy} + F_{\sigma y}, \tag{6}$$

$$\rho \frac{\partial v_z}{\partial_t} + \rho v_x \frac{\partial v_z}{\partial_x} + \rho v_y \frac{\partial v_z}{\partial_y} + \rho v_z \frac{\partial v_z}{\partial_z} = -\frac{\partial p}{\partial z} + \nabla \cdot (\mu \nabla v_z) + G_z + S_{vz} + F_{\sigma z}, \tag{7}$$

where: p is the density, kg/m^3; t is the time, s; p is the pressure, N/m^2; μ is the viscosity, kg/m · s; and G, S_v, F_σ are the sources, kg/m^2· s^2.

2.4.6. Conservation of energy

$$\rho c_p \frac{\partial T}{\partial t} + \rho c_p \left(v_x \frac{\partial T}{\partial x} + v_y \frac{\partial T}{\partial y} + v_z \frac{\partial T}{\partial z} \right) = \nabla \cdot (k \nabla T) + \dot{q}_v + S_h, \tag{8}$$

where: ρ is the density, kg/m^3; c_p is the specific heat capacity, J/(kg·K); T is the temperature, K; t is the time, s; v_x, v_y, v_z are the velocity components in x, y, z directions respectively, m/s; k is the thermal conductivity, W/(m·K); $\dot{q}_v$ is the volumetric heat source, W/m^3; S_h is the phase change latent heat source term, W/m^3.

3. Simulation and comparative study of the heat transfer process of snow melting in turnouts

3.1. Simulation model construction

A three-dimensional transient heat transfer model is developed to evaluate the snow-melting performance of two heating methods. Taking the UIC 60 rail type as an example, the heating elements are all 1 m in length, and the heating strip power is set at 500 W/m. A coupled physical model of 'heat source-rail-air' is established in Fluent software for simulation analysis. This study models both the traditional electric heating and the novel induction heating device based on their actual structures. To simplify the computation process and enhance simulation convergence, the model undergoes moderate simplification, and boundary conditions are defined. This includes neglecting thermal resistance at contact surfaces and the impact of air humidity on heat transfer within the turnout, as illustrated in Fig. 6. For result comparison with experimental data, the initial system temperature is set to 296 K. The base boundary is designated as an adiabatic boundary with heat transfer flux (q = 0 W/m^2). The lateral boundary is configured as a pressure outlet type with (P = 101 kPa), while the free surface is a convection-radiation composite boundary. The ambient temperature matches the initial temperature. Additionally, the air in the model is treated as an incompressible ideal gas.

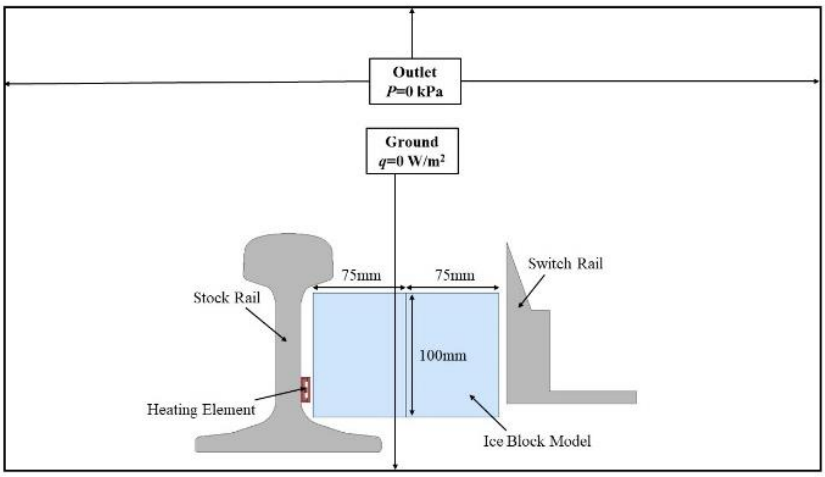

Fig. 6. Air domain and boundary conditions in the simulation model

3.2. Phase transition equivalent model

Given that ice and snow melting involves phase transitions, which are extremely complex and computationally intensive, this study adopts an approximate approach to simplify calculations while ensuring that the temperature field, heat flux, and time response are as close to real conditions as possible. Existing research has proposed various approximate methods for addressing phase transition problems, including: the equivalent specific heat method, which indirectly accounts for the effect of latent heat by introducing an equivalent specific heat within the phase transition

temperature range to avoid the complex calculations associated with interface tracking; and the enthalpy method, which implicitly incorporates latent heat effects into the energy equation through the relationship between enthalpy and temperature, achieving higher-precision heat conservation.

This study employs an equivalent alternative model to simplify calculations. A solid object with material properties identical to ice is selected as the subject, assumed to remain in a solid state without undergoing phase transition [16]. Simulation scenarios are divided into three conditions: a) complete snow-cover condition, where the ice cross-section measures 150×100 mm^2 with a volume proportion of 100%, simulating full snow accumulation between the base rail and switch rail; b) partial snow-cover condition, with an ice cross-section of 75×100 mm^2 and a volume share of 50%, reflecting uneven snow distribution; c) no-snow condition, where the volume share is 0%, indicating no snow presence between the base rail and switch rail.

For the first two scenarios, calculations terminate when the ice boundary temperature reaches 0°C (the critical phase transition temperature). In the third scenario, the air temperature between the base rail and switch rail must reach 0°C. This assumption reduces computation time compared to models incorporating phase transitions. Material parameters for each simulation component are detailed in Table 1.

Table 1. Thermal properties of materials

Structures	**Steel**	**Electric heating strip**	**Induction coil**	**Heating plate**	**Core**	**Magnetic**
Materials	U71Mn	SUS304	Copper	SUS430	MnZn	AlNiCo
Density/(kg·m^{-3})	7 920	7 930	8 933	7 700	4 900	7 300
Specific heat capacity/J/(kg·°C)	475	500	385	460	475	400
Thermal conductivity/W/(m·°C)	40	16	400	26	4	15

3.3. Analysis of simulation results

Figures 7, 8, and 9 present the temperature fields derived from transient solutions under varying working conditions, allowing visual observation of hot air diffusion.

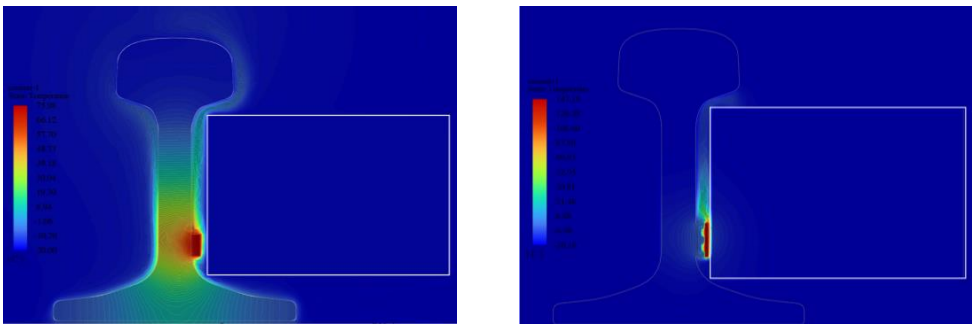

(a) (b)

Fig. 7. Temperature contour map depicting 100% volumetric coverage: electric heating (a); novel induction heating (b)

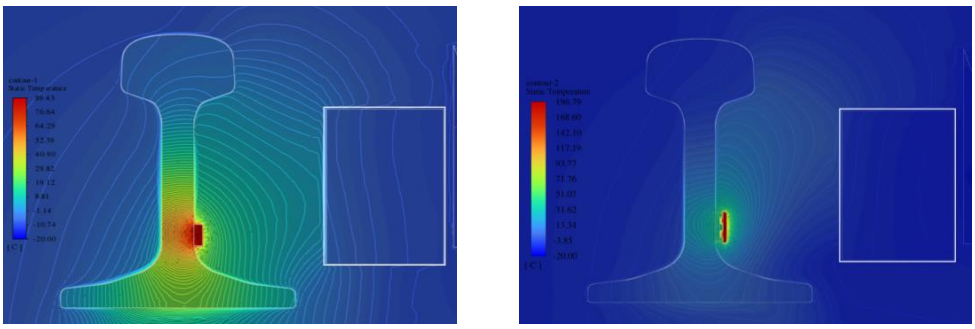

(a) (b)

Fig. 8. Temperature contour map depicting 50% volumetric coverage: electric heating (a); novel induction heating (b)

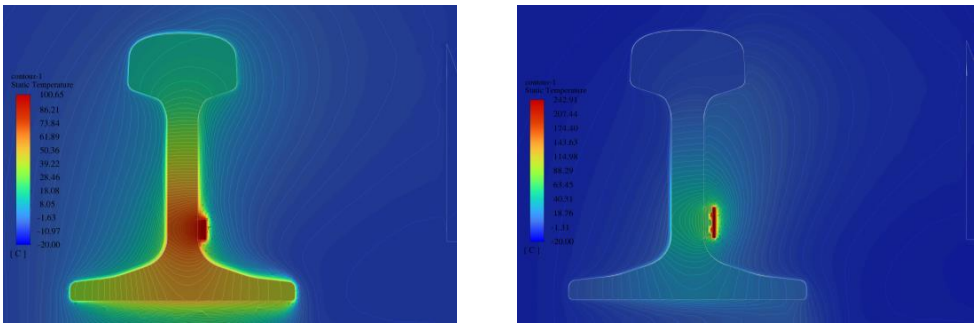

(a) (b)

Fig. 9. Temperature contour map indicating 0% volume fraction: electric heating (a); novel induction heating (b)

The time was normalised as follows:

$$t_s = t_{\text{real}} 100\% / t_{\max}, \tag{9}$$

where t_s is the normalised time, t_{real} is the time required to raise the ice boundary to 0°C for each case, and $t_{\max}$ is the longest time recorded in the conducted simulations. Results are presented in Table 2.

Table 2. Normalization schedule

Percentage by volume	**Electric heating/t_s**	**Novel induction heating/t_s**
100%	0.13	0.03
50%	0.42	0.21
0%	1.00	0.71

Based on the comparison of normalised times, the heating performance of the two methods under different ice volume ratios is analysed. At a 100% volume ratio, the normalised time for traditional electric heating is 0.13, whereas that for the novel induction heating is 0.03. This

indicates a significant reduction, with the novel induction heating requiring 76.9% less time to reach 0°C at the ice boundary compared to electric heating. As the volume ratio decreases, the normalised time difference between the two methods narrows. At a 0% volume ratio, the novel induction heating remains 29% faster than electric heating, retaining its performance advantage.

4. Experimental validation and performance optimisation

4.1. Construction of the experimental platform

To address the discrepancy between the ideal contact state of the heating element and the rail surface, and the actual contact thermal resistance in the simulation model, this experiment applies a thin layer of thermally conductive silicone grease (thermal conductivity of 4 W/(m·K)) at the contact interface to effectively reduce thermal resistance. The temperature acquisition system employs an AT4716-type high-precision multi-channel pyrometer. As shown in Fig. 10, the experimental setup includes two temperature measurement points each at the rail waist, rail foot, and rail head within the heating strip and rail. Experimental data are averaged, while three additional points are placed in the air region, corresponding to positions near the rail head, heating strip, and rail foot.

To ensure comparability between experimental data and numerical simulations, the finite element model incorporates identical virtual measurement points, establishing a spatially corresponding temperature field verification system.

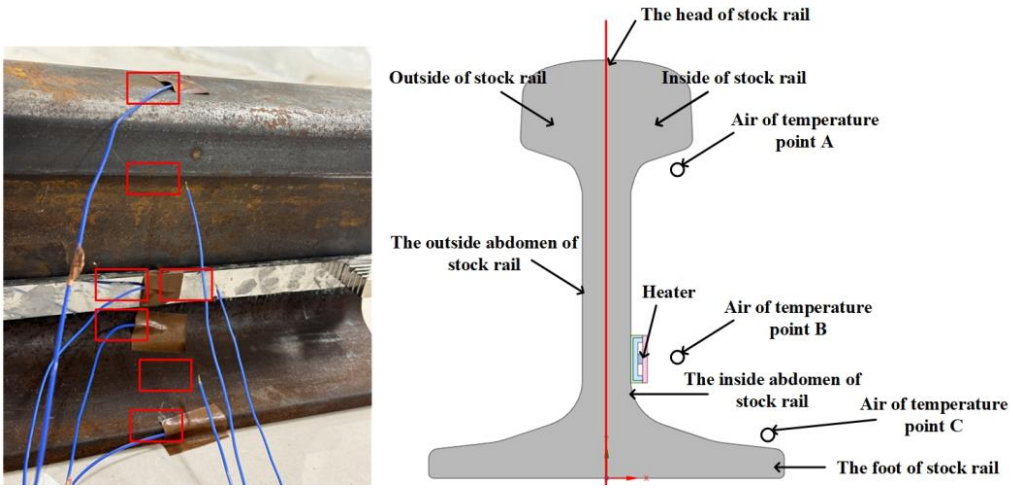

Fig. 10. Schematic diagram of temperature measurement points

4.2. Comparison of steady state temperature rise characteristics

The steady-state temperature rise test was conducted at 23°C under normal, ice-free conditions to validate the model's accuracy by comparing simulation and experimental data. As illustrated in Fig. 11, solid lines represent the experimental group, and dashed lines denote the simulation group.

In the traditional electric heating experiment, thermal equilibrium is achieved after approximately 12 000 seconds, with the heating strip reaching 228°C, and the rail waist, rail foot, and rail head recording 100°C, 84°C, and 84°C, respectively. In contrast, the simulation stabilises after 19 000 seconds, with temperatures of 215°C, 112°C, 94°C, and 90°C for the respective components. Comparison reveals that the experimental heating strip and air temperatures exceed simulated values by about 6.1% and 2.9%, respectively, while the average rail temperature is 9.3% lower than the simulated result.

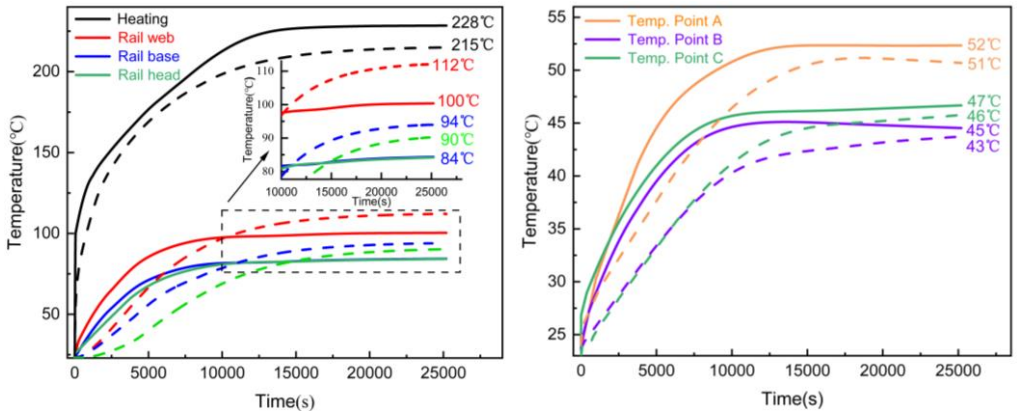

(a) (b)

Fig. 11. Comparison of experimental and simulated temperature rise in electric heating processes: heating strip and rail section (a); air region (b)

As illustrated in Fig. 12, in the novel induction heating mode, the experimental group reaches steady state after 10 000 seconds, with the heating strip temperature rising to 374°C. The rail waist, rail foot, and rail head record 93°C, 82°C, and 78°C, respectively. The simulation model stabilises after 20 000 seconds, yielding a heating strip temperature of 336°C, with corresponding rail temperatures of 97°C, 93°C, and 81°C. The experimental heating strip and air temperatures slightly exceed those of the simulation, while rail temperatures are relatively lower. The overall relative errors between the two datasets remain below 15%, with a maximum error of 11.8% and a minimum of 3.7%. This consistency validates the numerical model against experimental data, providing robust support for further investigations.

This alignment stems from the simulation model assuming idealised close joints between elements, whereas microgaps and thermal resistances are present in real experiments. Unlike conventional electric heating, where the track itself is the primary heat receiver in the absence of ice or snow, the novel induction heating incorporates a heating plate backed to the base track. This design leverages the optimised E-core structure and low-conductivity materials to create an adiabatic boundary layer, establishing a directional heat flow control mechanism. This structural innovation significantly alters thermal energy distribution. Numerical simulations indicate that the induction heating plate's steady-state temperature is 56.3% higher than that of the traditional resistive type, with average rail temperatures of 98.7°C and 90.3°C, respectively, reducing the temperature gradient by 8.5%. Experimental data corroborate this trend, showing a 64.0% increase

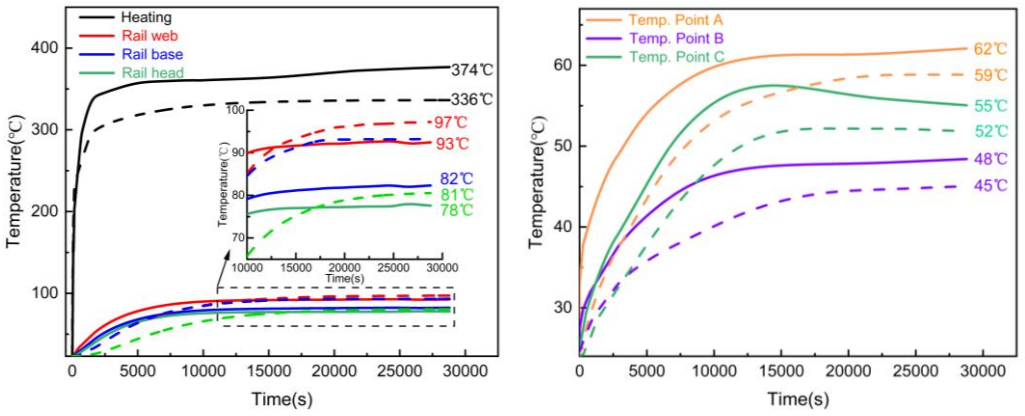

(a) (b)

Fig. 12. Comparison of experimental and simulated temperature rise in novel induction heating processes: heating plate and rail section (a); air region (b)

in the heating plate temperature, with average rail temperatures of 89.3°C and 84.3°C, a reduction of 5.6%. Under the novel induction heating method, the air temperature between the base rail and switch rail rises by 15% compared to traditional heating, enabling more heat to be utilised for turnout ice melting, consistent with theoretical analysis.

4.3. Comparative experimental study of snow melting effect

Ice melting tests were conducted in a laboratory at an ambient temperature of 23°C to compare the melting rates of two heating methods. To account for potential interference from elevated room temperatures on the heating device's melting effect, a control group was established without a heating device. This group monitored mass changes and temperature distribution in real time using a high-precision electronic scale and a temperature recorder. The ice melting rate was assessed over 2 hours, with ice cube weights recorded every 300 seconds. Each group provided 25 data sets, and the slope from linear fitting determined the melting rate, with results presented in Fig. 13.

In the ice melting test, the blank control group required 11 880 seconds to melt 2 200 g of ice, yielding a melting rate of 0.101 g/s. The conventional electric heating group and the novel induction heating group reduced this time to 6 940 seconds (0.173 g/s) and 5 910 seconds (0.203 g/s), respectively. The latter group's melting rate was 0.4 times higher than the former.

To simulate natural snow conditions and evaluate melting rates, 1 100 g of homogeneous crushed ice served as the test object. The time required to fully melt this mass under three different conditions was recorded, with results shown in Fig. 14.

In the snow-melting test, using 1 100 g of crushed ice samples, the blank group required 2 400 seconds to melt (0.458 g/s). This was reduced to 1 080 seconds (1.018 g/s) and 750 seconds (1.467 g/s) for the electric heating and novel induction heating groups, respectively. The novel induction heating increased the melting rate by a factor of 0.8 compared to the traditional mode, achieving an efficiency gain of 44.0%.

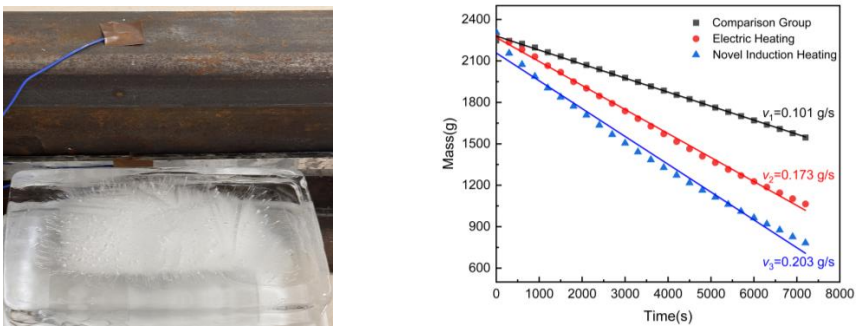

(a) (b)

Fig. 13. Ice melting rate measurement: ice melting test (a); ice melting rate comparison (b)

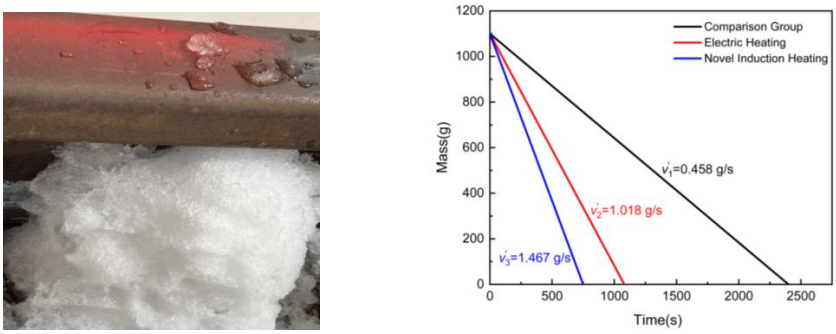

(a) (b)

Fig. 14. Snow melting rate measurement: snow melting test (a); snow melting rate comparison (b)

Based on the time-energy conversion model analysis, the novel induction heating system achieved energy optimisation of 29.1% and 41.8% in ice-melting and snow-melting tests. Respectively, this result is consistent with previous research findings: Robert *et al*. demonstrated that induction devices operating at frequencies of 40–70 kHz consume only 30–60% of the energy used by resistive heaters [2]. In summary, the unique electromagnetic-thermal synergistic effect of the novel induction heating concentrates more energy in the working area, significantly enhancing energy utilisation compared to traditional electric heating. This directional energy transport characteristic maintains a 30–40% efficiency advantage under mixed-phase conditions involving snow, frozen ice and liquid water coexistence.

4.4. Simulation verification of thermal efficiency improvement based on composite thermal structures

In practical switch snow-melting scenarios, heat generated by heating elements during operation is dissipated through the outer surface of rails. This heat loss is not utilised for actual snow-melting processes and thus constitutes ineffective heating. Through thermodynamic simulation

analysis, various parameters in the model were thoroughly investigated and evaluated. The results indicated that the emissivity of the heat source is one of the key parameters influencing the model performance. Specifically, the surface emissivity of the heat source acts as the core control variable determining thermal field distribution, and its settings exhibit a significant positive correlation with radiant energy density – this correlation is characterised by uniqueness. Related studies have also confirmed that increasing the amount of radiative materials can effectively enhance the emissivity of the heat source.

To mitigate heat loss, this study proposes an improved composite thermal structure: an insulation layer (with a thermal conductivity of $\lambda = 0.028$ W/(m·K)) is applied to the outer side of rails to suppress external heat dissipation. Concurrently, a radiation enhancement structure (with an emissivity of $\varepsilon = 0.92$) is installed on the inner side to promote directed heat transfer. A schematic diagram of the thermal structure design and the temperature distribution contour map are presented in Fig. 15. Steady-state simulations were conducted at identical temperature-measuring points for comparison, providing robust data support for subsequent improvements to heating elements.

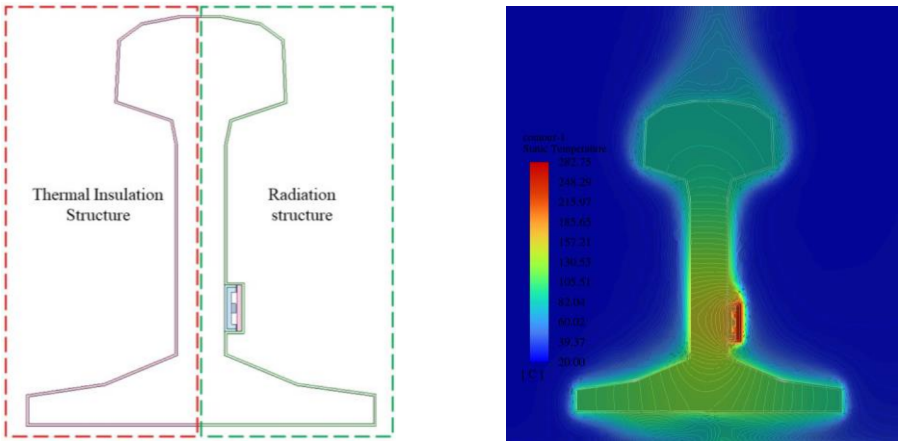

(a) (b)

Fig. 15. Composite thermal structure design and temperature distribution clouds: schematic diagram of composite thermal structure (a); temperature distribution cloud (b)

Temperature variations after the application of the composite structure are summarised in Table 3. Following the installation of the insulation and radiation structures, the temperature of the heating plate decreased by 54°C (a relative change rate of 16%), which effectively reduces overheating losses. The temperatures of the rail head, rail foot, and inner rail web all exhibited a decreasing trend, with relative change rates of 5%, 6%, and 5%, respectively. In contrast, the temperatures of the outer rail web and the surrounding air increased, with the average change rate in the air region reaching 7%. These results demonstrate that installing a radiation enhancement structure on the inner side of the heating strip and stock rail can improve thermal radiation transfer in the working area, while applying insulation material to the outer side of the stock rail reduces external heat loss. Through these synergistic measures, the energy utilisation efficiency of switch snow-melting equipment can be significantly improved, thereby further achieving energy conservation.

Table 3. Comparison table of temperature change of each part after optimized design

	Heating plate	**Rail head**	**Rail base**	**Inside of the rail web**	**Outside of the rail web**	**Temp. Point A**	**Temp. Point B**	**Temp. Point C**
ΔT/°C	–54	–4	–6	–5	+9	+4	+6	+2
Rate of change	–16%	–5%	–6%	–5%	+8%	7%	11%	4%

5. Conclusion

This paper presents a novel turnout snow-melting system based on electromagnetic induction heating. Through theoretical analysis, numerical simulation, and experimental validation, the limitations of existing electric heating systems are systematically examined. A composite thermal structure design is proposed to enhance directional heat transfer, offering theoretical and technical support for improving the thermal efficiency of railway turnout snow-melting systems.

This preliminary study also identifies several areas requiring further investigation. The phase transition process is computationally intensive; thus, the study focused on the semi-molten state of ice to simplify calculations, highlighting the need for more accurate modelling approaches in future work. Experimental testing was limited to laboratory conditions under ambient temperatures due to regional climate constraints, excluding real-world environmental factors such as sub-zero temperatures, wind, and precipitation, which influence snow-melting performance.

Furthermore, the long-term durability of components under prolonged high-frequency operation – including thermal fatigue and oxidative degradation – as well as manufacturing and maintenance costs, were not evaluated. Field trials and accelerated ageing tests would be valuable to systematically assess the lifecycle performance and economic viability of the system and its critical components.

References

[1] Liu H.X., Zhao X.F., *Tram Winter Operation Safeguard in Severe Cold Areas*, Urban Mass Transit, no. S1, pp. 74–77, 81 (2021), DOI: 10.16037/j.1007-869x.2022.S1.017.

[2] Żelazny R., Jabłoński P., Szczegielniak T., *Operation of the Prototype Device for Induction Heating of Railway Turnouts at Various Operating Frequencies*, Energies, vol. 14, 476 (2021), DOI: 10.3390/en14020476.

[3] Su R., Li Z.M., *Scheme of Intelligent High-Speed Railway Point Heating System*, Railway Signalling & Communication Engineering, vol. 19, no. 10, pp. 24–29 (2022).

[4] He Q., Li Z.L., Huang Y. *et al.*, *Construction and Analysis of heat transfer model for Electric Heating Elements in Switch Snow Melting System*, Journal of Railway Science and Engineering (2024).

[5] Szychta E., Szychta L., *Testing of Turnout Resistance and Induction Heating in Climatic Chamber*, 2021 IEEE 19th International Power Electronics and Motion Control Conference, Gliwice, Poland (2021), DOI: 10.1109/PEMC48073.2021.9432523.

[6] Ning Y.M., Yan H.W., *Research on Optimization of Engineering Design Standards of Snow Melting Devices for Railway Turnouts*, Railway Signalling & Communication Engineering, vol. 20, no. 1, pp. 7–13 (2023).

[7] Kirawanich P., *A Numerical Technique for Estimating High-Frequency Radiated Emissions from Railway System*, IEEE Transactions on Electromagnetic Compatibility, vol. 63, no. 2, pp. 463–473 (2021), DOI: 10.1109/TEMC.2020.3010256.

[8] Zhang P.F., Wang D.C., Cheng P. *et al*., *Finite Element Simulation of Induction Heating 65Mn Strip Steel Based on Electromagnetic-Thermal Coupling*, Materials Review, vol. 36, no. 12, pp. 150–155 (2022), DOI: 10.11896/cldb.20110208.

[9] Li Z.F., Hu J.C., Huang M.S. *et al*., *Load Estimation for Induction Heating Cookers Based on Series RLC Natural Resonant Current*, Energies, vol. 15, no. 4, pp. 1294–1313 (2022), DOI: 10.3390/en15041294.

[10] Yan S.C., *Application of Electromagnetic Induction Heating Technology in Snow Melting and De-Icing Operation for Switches*, Electric Railway, vol. 33, no. 4, pp. 96–99 (2022), DOI: 10.19587/j.cnki.1007-936x.2022.04.019.

[11] Oh H.S., Park C.B., Lee S.H., *A Study on De-icing for Railway Turnouts Using 250kHz-200w-Class Induction Heating System*, AIP Advances, vol. 9, 125229 (2019), DOI: 10.1063/1.5129857.

[12] Plumed E., Lope I., Acero J., *Induction Heating Adaptation of a Different-Sized Load with Matching Secondary Inductor to Achieve Uniform Heating and Enhance Vertical Displacement*, IEEE Transactions on Power Electronics, vol. 36, no. 6, pp. 6929–6942 (2021), DOI: 10.1109/TPEL.2020.3038604.

[13] Szychta L., Szychta E., Kiraga K., *Efficiency of Induction Heating of Rails with Oblong Heaters*, Telematics in the Transport Environment, vol. 329, pp. 328–333 (2012), DOI: 10.1007/978-3-642-34050-5_37.

[14] Flis M., *Energy Efficiency Analysis of Railway Turnout Heating System with a Melting Snow Model Heated by Classic and Contactless Heating Method*, Archives of Electrical Engineering, vol. 68, pp. 511–520 (2019), DOI: 10.24425/aee.2019.129338.

[15] Vajdi M., Moghanlou F.S., *A Review on the Comsol Multiphysics Studies of Heat Transfer in Advanced Ceramics*, Journal of Composites and Compounds, vol. 2, no. 2, pp. 35–43 (2020), DOI: 10.29252/jcc.2.1.5.

[16] Flis M., *Contactless Turnouts' Heating for Energy Consumption Optimization*, Archives of Electrical Engineering, vol. 69, no. 1, pp. 133–145 (2020), DOI: 10.24425/aee.2020.131763.